A novel paradigm for the fabrication of highly uniform nanowire arrays using residual stress patterning

Zhi Zhao[a], Nan Wang[b], Hanqing Nan[a], Li Shen[a], Colm Durkan[b], Ximin He[a, c]

[a] School for Engineering of Matter, Transport and Energy, Arizona State University, Tempe, AZ 85281, USA

[b] The Nanoscience Centre, University of Cambridge, 11 J. J. Thomson Avenue, Cambridge CB3 0FF, United Kingdom

[c] The Biodesign Institute, Molecular Design and Biomimetics Center, Arizona State University, Tempe, AZ 85281, USA

Abstract

Patterned low-dimensional (1-D or 2D) nanomaterials have recently drawn tremendous attentions with their unique properties. To realize their wide potential applications in electronics, sensing and energy storage, it is critical yet still challenging to fabricate highly uniform 1-D material arrays (e.g. nanowire arrays) that simultaneously feature high resolution, large scale and tunable geometric parameters. Herein, we report a novel method for fabricating large-area, highly aligned nanomaterials using a one-step residual-free nanopatterning via pressure-induced instabilities in thin polymer films. We demonstrate the fabrication of highly tunable, vertically aligned single-crystal zinc oxide (ZnO) nanowire (NW) arrays via low-temperature hydrothermal synthesis on arbitrary substrates. The dimensions, locations and orientations of ZnO NWs are precisely controlled through the spatial confinement effect of the spontaneously formed polymer masks. The high quality of the as-prepared NW arrays have been revealed by the systematic characterization of the morphology, crystalinity, and piezoelectric properties of single ZnO NWs. Conductive atomic force microscopy (cAFM) measurements show Schottky barrier characteristics in the I-V curves and a clear registration of the detected current signal with individual NWs. Mechanically-induced currents are observed to change with the deformation magnitude of NW, directly indicating the generation of piezoelectricity. This work provides a novel universal paradigm for patterned 1-D nanomaterial fabrication and opens up unprecedented opportunities for more design innovations and applications in nano-devices.

KEYWORDS: Nanopatterning, Residue-free, 1-D materials, ZnO nanowires, Piezoelectricity

1. Introduction

Nanomaterials such as one-dimensional metal (oxide) nanowires or two-dimensional atomic layers have been identified as useful building blocks for nanoscale electronic devices, when they are grown or aligned in a controlled structure. [1-4] Zinc oxide (ZnO) nanowires (NWs), for example, have attracted extensive research interest because of their semiconducting-piezoelectric dual properties, [5] direct bandgap and large exciton binding energy, [6,7] and the diversity of synthetic and processing strategies. [8] ZnO NWs grown perpendicular to the substrate with uniform morphology and good alignment are particularly useful in applications including antireflection optics, ZnO-polymer hybrid photovoltaic devices, and chemical/biochemical sensors. [9-11] The foremost promising application of ZnO NWs in piezoelectricity generators is based on large-area highly-aligned array of piezoelectric NWs, which convert mechanical energy to electricity when they are uniaxially compressed. [12,13] Thus the controlled growth of well-aligned nanomaterials in predetermined configurations is the critical prerequisite for realizing the advanced functions of many 1-D materials. [14-22] In particular, the morphology control of NW materials includes NW shape, diameter, height and crystallinity, as well as the arrangement of NW arrays, such as the periodicity and symmetry of NWs arrays. Consequently, there is a strong demand for nanopatterning schemes compatible with a wide variety of geometric parameters and device fabrication processes. [23]

Wet chemical synthetic routes at low temperature (< 100℃) is favorable for their compatibility with broad choices of substrates and electronics manufacturing in comparison with high-temperature (> 600 ℃) vapor-liquid-solid (VLS) growth methods, [24-27] but the diameter and orientation of the as-grown NWs vary significantly. [28] Therefore, several patterning methods have been employed to confine NW growth via masking. For example, patterned photoresist has been used to define nucleation regions to produce single crystal ZnO disks of 4-μm width with an aspect ratio < 0.5, which as the building blocks created light emitting diodes and UV photovoltaic cells. [29] Recently, wafer-scale aligned NWs have been fabricated with polymer masks patterned by laser-interference lithography. [30, 31] Moreover, electron beam lithography (EBL) has been used to produce well-aligned patterned ZnO nanowire arrays. [32] A common issue in those methods is the potential contamination from the post-development residue on

substrates, [33] which may affect the uniformity of NWs' alignment. Meanwhile, lack of tunability is another drawback of those methods, in which only one pattern can be generated from each photomask. In addition, the patterning resolution is limited for photolithographic methods, while EBL is not feasible for economic large-scale fabrication. The current challenge is how to develop a residue-free, tunable mask fabrication technique that simultaneously satisfies the resolution and large-scale requirement in ZnO NWs synthesis.

We previously reported a non-conventional nanopatterning technique based on pressure-induced instabilities in polymer thin films. [34] Herein, we have employed this technique to synthesize highly uniform, vertically aligned ZnO NWs at nanometer resolution. In contrast to conventional lithography techniques, our method is able to produces patterns with residual-free surfaces in a single step. By controlling the patterning parameters or applying post thermal annealing, the surface pattern sizes can be tuned between ~20 nm and hundreds of nm. With this technique, we have demonstrated that ZnO NWs of various sized can be prepared from a single stamp. The as prepared ZnO NWs showed characteristic semiconducting-piezoelectric dual properties and promises for future electronic applications. As our method obviates the subsequent etching or developing steps required in other lithography techniques, which significantly simplifies the fabrication process and reduces the cost. We believe this strategy provides a universal, cost-effective paradigm applicable to many other nanomaterials.

2. Material and methods

2.1 Polymer mask fabrication

Detailed polymer patterning method has been described in our previous publication. [34] The polymer that we used in this work was polystyrene (PS, Mw 50k, PolyScience Inc.). Briefly, PS film spun cast onto a single crystal ZnO (sc-ZnO) substrate (Semiconductor Wafer, Inc.) or a textured ZnO seed layer chemically grown on a Si substrate [10] was approached by a fluorinated Si stamps containing 2D conical-shaped sharp tip arrays, with tip radius of < 10nm, tip length of 0.5-1.5 μm, and periodicity of 2.12 μm (Figure 1). When the stamp gently touched the film surface by applying a mild pressure for tens of seconds, hollow circular pattern formed simultaneously under areas in contact with the stamp. In order to obtain proper hole size and well define the orientation of ZnO NWs grown from the substrate, the thickness of PS film was

controlled to be 50-80 nm. Particularly, the 50 nm-diameter circular hole array was made by imprinting a freshly prepared 60 nm thick PS film at 60 ℃ under 3 bar pressure for 30 seconds. In order to control the NW diameter, subsequent thermal annealing was applied on the patterned PS film containing 50 nm holes at 75 ℃ for 15 and 30 sec in air to tune the opening diameters to 100 and 300 nm.

2.2 Growth of ZnO NW

The ZnO NW arrays were synthesized in the nutrient aqueous solution of 0.2-1 mmol/L 1:1 zinc nitrate hydrate ($Zn(NO_3)_2 \bullet xH_2O$) and hexamethylenetetramine (HMTA). The substrates were vertically placed in the nutrient solution. The whole system was heated in a water bath up to 96 °C for 20 and 120 minutes respectively for growing the 0.65 and 3.2 μm long NWs.

2.3 Morphology and crystal structure characterization

The morphology of the as-produced ZnO NW arrays were studied by SEM (Variable pressure, Leo) and AFM (Molecular Force Probe MFP-3D, Asylum Research) at tapping mode. The crystal structures of the ZnO NWs were studied by TEM and XRD (Philips/Panalytical PW3050/65 X'Pert). TEM samples were prepared by transferring the as-grown ZnO NWs to a carbon film on a copper grid. A Phillips CM30 microscope, equipped with a LaB6 thermionic gun and a 300 keV acceleration voltage, was used to perform conventional TEM including bright field, dark field and diffraction on individual ZnO NWs.

2.4 Electrical properties characterization

The morphology and piezoelectric properties of the as-produced ZnO NW arrays were studied by using the conducting AFM (Molecular Force Probe MFP-3D, Asylum Research) with a Pt/Ir-coated Si probe (tapping probe, probe tip height: 10~15 μm, tip radius of curvature:10~20 nm, cantilever: Si, resistivity: 0.01-0.02 Ωcm, Resonance Frequency: 204-497 kHz, spring constant: 0.1 N/m, Nanosensors). The I-V spectroscopy at contact mode was recorded under dark conditions at a voltage sweep rate of 3 mV/s using a constant normal force of 6 or 8 nN. The piezoelectric responses via single NW manipulation or during AFM scanning at contact mode were measured without any external voltage. When the tip scanned over the top of the ZnO NWs, the position of the tip was adjusted according to the surface morphology and local contacting force. A metal pin fixed on the metal sample holder was used to fix the sample and

connect the substrate with the measurement circuit for their electric contact. Silver paint was applied between the bottom of ZnO substrate and the sample holder to make sure a good electric contact. The electrode at the base of the sample was grounded. For single NW piezoelectric property measurements, multiple experiments (20-30 times) were performed with the cAFM cantilever tip pressing at all positions (position 1, 2, 3 and 4) in order to investigate the repeatability and reliability of the cAFM piezoelectric experiments.

3. Results and Discussion

3.1 Morphology of ZnO nanowires

Perfectly aligned and highly uniform ZnO NW arrays, as shown in Figure 2, were successfully fabricated on sc-ZnO substrate using this approach, with each opening containing a single NW. The TEM images have shown very good crystallinity and a close match between the (0001) crystal plane of the sc-ZnO substrate and the NW lattice. Importantly, the polymer surrounding the hole, with a slightly elevated rim induced by the patterning procedure, provided effective spatial confinement to the NW growth and limited the number of NWs grown from each opening. For comparison, ZnO NW arrays were also synthesized on ZnO seed layers deposited on Si substrates (Figure S1), interestingly with multiple NWs growing out of each opening instead. This comparison indicates that the initial crystallinity of ZnO played the key role in determining the morphology of the patterned ZnO NW array, especially the orientation and number of NWs in a single opening (Figure S1).

Figure 2a-c shows the top-view (Figure a1-c1) and 45° tilted-view (Figure a2-c2) SEM images of highly uniform ZnO NW arrays grown on sc-ZnO substrates. As the opening size increased from 50 to 100 and 300 nm, the NW top diameters increased from 144 nm to 211 nm and 380 nm, respectively, and the bottom diameters from 400 nm to 560 nm and 600 nm; while the height remained the same at 3.2 μm for 120 minute growth and 0.65 μm for 20 minute growth, as measured by AFM (Figure 2e1-e3). Their shape and sizes were very uniform, with only 0.8% standard deviation (STD) for their diameters in the case of the NWs grown from 300 nm openings. The NWs are regular hexagonal pillars with a uniform conical shape, whose diameter gradually decreased from the bottom to the top (approx. half of the bottom size). The top/bottom outer diameter of the NWs, grown from the 100 nm openings for example, was 211/560 nm

respectively. It should be noted that their diameters exceed the size of the openings in polymer film as a result of overgrowth in lateral directions. [29] Using the polymer mask, the NWs were placed with a minimal positional deviation of 0.9% (18 nm STD for the 2.12 um pitch), calculated by measuring the center-to-center distance between the ZnO NWs (Figure 2e1-e3). Additionally, the panoramic view image in Figure 2f reveals that the area of uniformly aligned NWs can reach 1×1 mm^2, showing the excellent large-scale patterning capability of our method.

The TEM diffraction patterns (Figure 2d2) indicate that the NWs are single crystalline with hexagonal symmetry, consistent with the wurtzite structure of ZnO. Together with the SEM images, we can infer that the NWs grow along the [0001] direction and are enclosed by six facets. [35] In the weak beam dark field image taken with a reflection $\boldsymbol{g}$=10-10, we observe the thickness fringes along the NW, as shown by the green arrow in Figure 2d1, which is due to the 2D projection of the crystal facet and indicates good crystalline quality of the NWs. Planar defects are also observed, as pointed out by the red arrows in Figure 2d1. The good morphology and crystallinity indicated that high-quality ZnO NWs were achieved during the synthesis and that the PS film, with a T_g of ~100 ^oC, survived the NW growth without deformation or decomposition. ZnO NW fabricated on ZnO seed layer-covered Si generally showed the same structure/crystallinity as those obtained from sc-ZnO substrate, with some slight difference in NW geometric parameters (Figure S2).

3.2 Characterization of Piezoelectric Property

The semiconducting-piezoelectric dual properties are characteristic for ZnO NWs and required for many applications. [5] It is highly desired that the patterned NWs are able to yield stable and uniform piezoelectric output current over a large surface area. To characterize the piezoelectricity of thus-prepared NW arrays, the electric responses to the mechanical deformation of the NW arrays were measured using cAFM. When the cAFM tip scanned across the as-grown ZnO NW array, the output current signals were simultaneously collected along with the height signals. The current was defined in such a way that positive current represented that the electrons moved from ZnO NWs into the AFM tip. [36] We observed regular current signals clearly registered to the NW location, as shown in Figure 3. The output current was almost identical for all the NWs, indicating that the consistently high quality of individual nanowires led to uniform piezoelectric properties across the sample. The current signals were comparable to the

(disordered) output signals from homogeneously grown ZnO NW arrays reported previously, [36-38] but the uniform bending distance recorded in the topography image (Figure 3a) was observed much more clearly. [39] From the output current, the ZnO NWs can be identified as n-type. [29, 36] The observed positive current was in line with theoretical studies on potential and electron distributions in bent ZnO NWs, where charge carriers were accumulated at the stretched side of the ZnO NW, while the electrons at the compressive side were largely depleted. [36, 37]

It is important to note that, despite the good matching between the topography and current, the measurement as above and also in previous reports involved complicated movements of both the cAFM tip and NWs: as the cAFM tip scanned laterally across such high aspect-ratio features, sudden vertical movements of the scanner were required to maintain the constant contact force. [36, 38, 39] Depending on the particular microscope used, this could induce both topographic and electrical artifacts. This inevitable problem, together with the complexity of the varying contact interface and mechanics in the lateral scan measurement, made the data analysis and explanation of the NW piezoelectric behavior complicated. [40] To avoid scanning-related artifacts, we further vertically compressed individual ZnO NWs with a constant force or bias to investigate their electrical and piezoelectric properties, as illustrated in Figure 4a. Since the measured current was produced without the interference from any lateral force as reported before, [38, 39] other complicating factors that might affect the analysis of the data, such as displacement current, [41] changes in capacitance/resistance of the tip-sample contact, and triboelectric effect, [42] could be ruled out.

All the single NW characterizations were performed with 330 nm-wide (top diameter) 3.2 μm-tall ZnO NWs. First, I-V curves of individual ZnO NWs were recorded (Figure 4 (a)). This I-V curve of a NW shows a typical Schottky contact behavior. [43] The rectifying behavior of the I-V curve indicates the existence of the Schottky barrier across the tip-nanowire, which is important for piezoelectric charge preservation. [44] From the I-V curves, we plotted $\ln|I| \propto |V|^{1/4}$, [45] and obtained a good linear relationship as shown in Figure S3. This result verifies that the piezoelectric potential is generated at the metal tip-semiconductor NW interface under external mechanical force, which has been known as piezotronic effect and utilized to fabricate strain-gated piezotronic transistor arrays with vertical ZnO NWs. [45, 46]

Based on this finding and using the same setup, we further studied the piezoelectric characteristics of single ZnO NW in the way as illustrated in Figure 5a right panel. A cAFM tip was repeatedly brought into contact at different positions on top of individual vertically aligned ZnO NWs without any bias applied. The current response and cantilever deflection upon vertically pressing at each position on NW top surface illustrated in Figure 5b were simultaneously recorded, as shown in Figure 5c1-c4. All measurements were repeated for 100 cycles and average data is presented with STDs in the range of 0.2-8%.

A control experiment was conducted on the substrate (position 0), with the AFM cantilever deflected by an identical amount as when on the top of a NW; no detectable current response (< 1 pA) was observed, as shown in Figure 5c0, which is consistent with the fact that no piezoelectricity was generated. In contrast, a few pA current was observed upon vertically pressing onto the center of the NW (position "1" as shown in Figure 5c1). When the tip is pressing slightly off-center (38 nm, position "2"), a higher current was observed at the moment when the cantilever deflection was 46 nm, and the current increased to 46-68 pA (56 pA in average) at a deflection of 80 nm, which corresponds to an applied force of 8 nN. When the tip was moved further towards the edge, the current response increased to 95 and 136 pA, at position "3" and "4", 76 and 114 nm away from the NW center. Such vertical pressing at a series of different positions on the NW top surface with precise distances from the center resulted in well-controlled deflection of NWs. This was indicated by the different deflections of the cantilever under the same pressing force (Figure 5c0-c4) and also previously observed from the bending distance recorded in the topography image (Figure 3a). The generation of output current directly and clearly revealed the piezoelectricity of ZnO NWs, which was in agreement with previous result obtained from laterally scanning across ZnO NWs. [29] The vertical loading generated dipoles in the bent NW, which in turn created a potential difference perpendicular to the axis of the NW. The clear position-dependence of output current we observed was attributed to the larger deformation of ZnO NW under off-center force. Such a property is highly valued and may be applied in sensing, high-resolution strain and pressure mapping, etc. The statistical data for different positions at 80 nm deflection were summarized in Table S1. Our results can be rationalized by a simple calculation on the relation of the piezoelectricity versus force applied on the center of the ZnO (see SI for more details). Briefly, the piezoelectric effect came from a change in the dimension of the NW under compression (note, we assume a vertical compression

for simplicity, rather than bending of the NW). By taking into account the Young's modulus, the aspect ratio of the NW, and the ZnO c-axis piezoelectric constant, we can plot the voltage output as a function of compressive force (Figure S4). The order of magnitude of the predicted voltage produced compares reasonably well with experimental data taken at 8 nN (after converting the current to voltage).

4. Conclusions

In conclusion, we have demonstrated how one-step residual-free nanopatterning in combination with hydrothermal synthesis under mild conditions can be used as a cost-efficient method to fabricate highly vertically aligned and uniform NW arrays with good positional and dimensional accuracy. As a proof-of-concept example, ZnO NW with top diameters ranging from 144 nm to 300 nm and lengths from 0.65 to 3.2μm were obtained with good crystallinity. The control over placement and synthesis of ZnO NWs greatly facilitated the study of electromechanical properties of individual ZnO NWs using cAFM. Large-area scanning yielded an output current pattern matching the vertical displacements of the AFM tip. Closer characterization of individual ZnO NW revealed that the increase in the bending of the NW induced by compressive force applied on the NW resulted in an increase in output current. The magnitude of the output current appeared to be related directly to the degree of NW bending determined by where and how hard the AFM tip pressed onto the NW. These comprehensive studies on synthesis, fabrication and characterization provide an ideal platform for further investigations into the fundamentals of many other types of 1-D materials and offer a route to incorporation NWs with desired electrical properties into large scale devices.

The perfect uniformity of the patterned 1-D nanomaterials, in terms of the geometric shape, diameter, height and crystallinity, would lead to highly uniform physical properties and functions such as the bending induced current. Particularly, a consistent electric power generated by uniaxially compressing highly aligned array of piezoelectric nanowire (e.g. ZnO, $PbZr_xTi_{1-x}O_3$, *etc*.) of the same height prepared by this method, would dramatically improve the feasibility and efficiency of using nanogenerators for powering mobile and even personal microelectronics. [47] Also, patterned and well aligned high aspect-ratio nanostructures grown in this way allows the precise control of the interaction between incident light and microstructures and thus help

improve optical function, such as the antireflection efficiency. [48] Controlling the spacing between nanostructure could solve the problem of insufficient infiltrating of conjugated polymers into the nanostructured semiconducting matrix when fabricating hybrid polymer photovoltaic devices. These well controlled arrays may serve as scaffolding for the deposition of other materials for an even wider range of applications. Such in-site growth control can be applied to a broad range of materials, including metals, metal oxides and polymers, which will aid the incorporation of nanomaterials into a variety of devices.

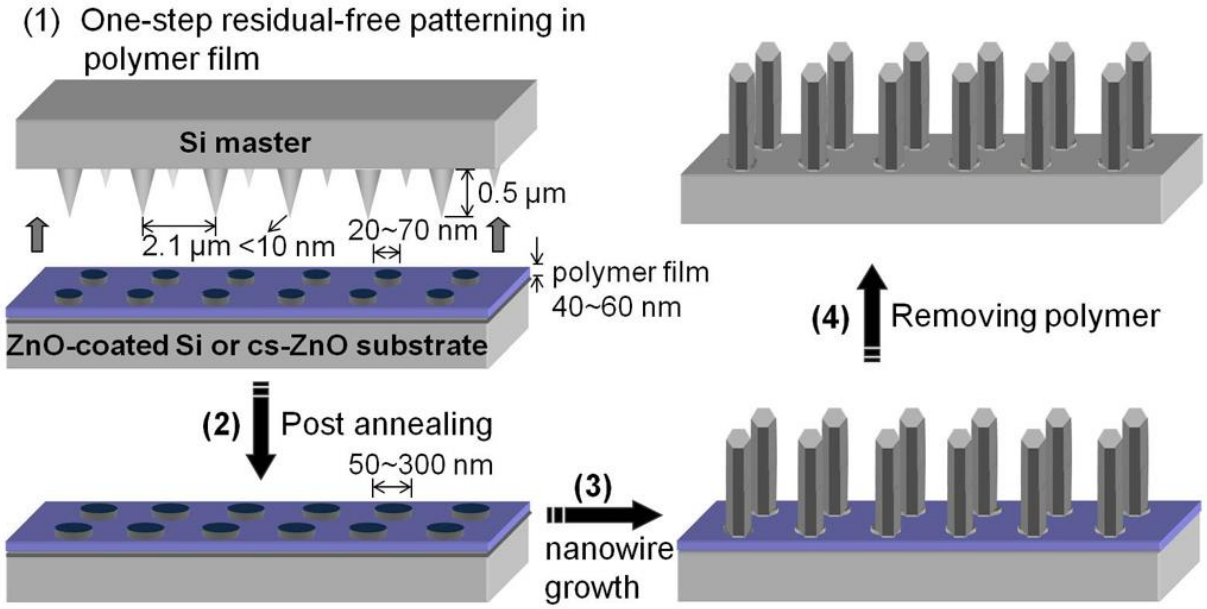

Figure 1. Schematic of the fabrication of 2-D patterned well-aligned ZnO NW arrays. **(1)** A 40-60 nm thick polymer film, spun cast on ZnO substrate, is approached by a fluorinated Si stamp containing conical-shaped sharp tip arrays, with tip radius of < 10 nm, tip length of 0.5 μm, periodicity of 2.1 μm. Stamp gently touches the film surface by applying a pressure of 3-5 bar. 20-70 nm diameter circular opening array forms under areas in contact with stamp. After 50-60 seconds, stamp is lifted from the film. **(2)** The diameter of the as-produced openings in polymer film was increased from 50 to 100 and 300 nm by using thermal annealing at 120 °C. **(3)** Growth of single ZnO NWs by hydrothermal synthesis. **(4)** Removing of the polymer film by soaking the sample in solvent.

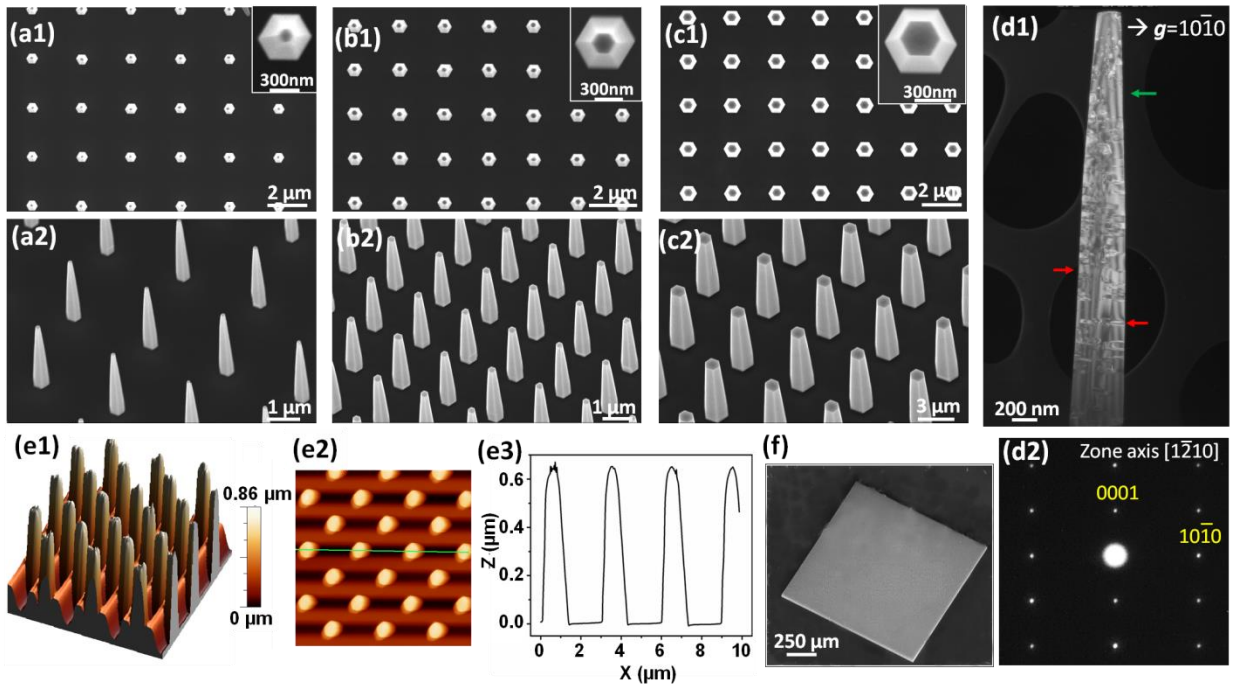

Figure 2. SEM **(a-c, f)**, TEM **(d)** and AFM **(e)** images of 2.12 μm pitch patterned nanowire arrays grown in 20 mmol/L nutrient aqueous solution for 20 minutes, on patterned ZnO crystal substrates. **(a1-c1)** are plane view images; (**a2-c2)** are 45°tilt view images, corresponding to **(a1-c1)**. The opening diameter in **(a)**, **(b)** & **(c)** is 50, 100 & 300 nm, respectively. **(f)** is the 45° tilt view panoramic SEM image of 1×1 mm patterned NW array, corresponding to **(c1)** and **(c2)**. **(d1)** is weak beam dark field TEM image of a NW grown identically for 120 minutes, with red arrows pointing out possible planar defects and green arrow the thickness fringes. Corresponding diffraction patterns taken on zone axis [1$\bar{2}$10] are shown in **(d2)**, with two typical diffraction spots labeled. **(e1-e3)** are (tapping mode) AFM 3-D height image, plane-view height image, and cross section profile of the NWs grown from 100-nm openings at identical conditions for 20 minutes.

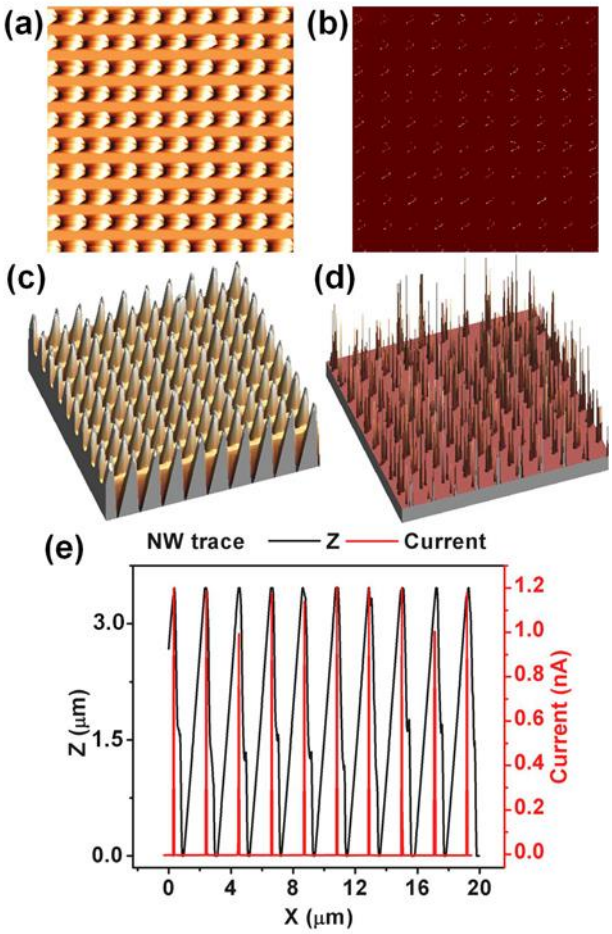

Figure 3. Topographic (a, c) and current (b, d) images of NW arrays as shown in Figure 2b2 in contact mode. The height and top diameter of the NWs are 3.2 μm and 250 nm, respectively. (c), (d) are 3D images of (a), (b) respectively. (e) is the corresponding topographic and current profiles. Scan area: 20 μm. Scan speed: 25 μm/s. The AFM data were analyzed using WSxM 4.0. [49]

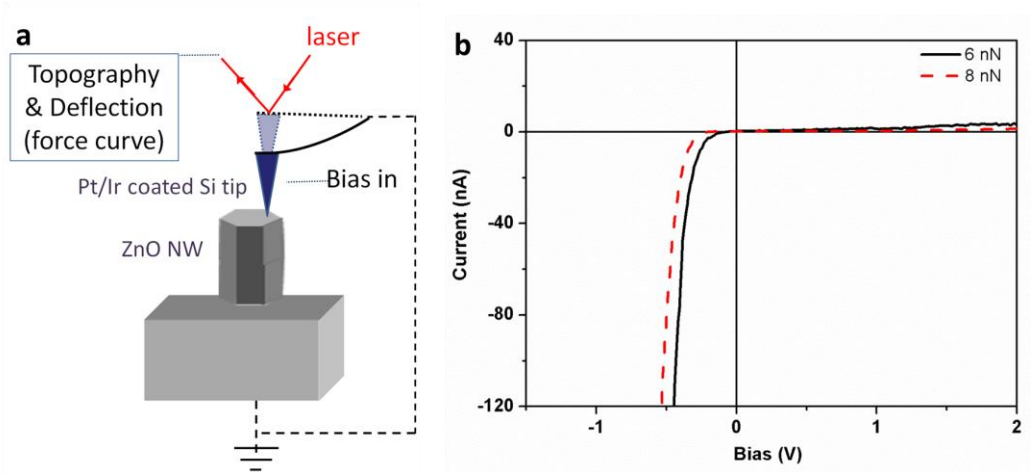

Figure 4 (a) Schematics of the cAFM measurement on individual ZnO NW **(b)** I-V curves obtained by aligning the AFM tip on the top of a ZnO NW (position 1) with applied force of 6 and 8 nN respectively and bias sweeping a cycle between -2~2 V: starting from 0 to 4, back to 0, and then to -4, finally back to 0 V. Rate: 3 mV/s.

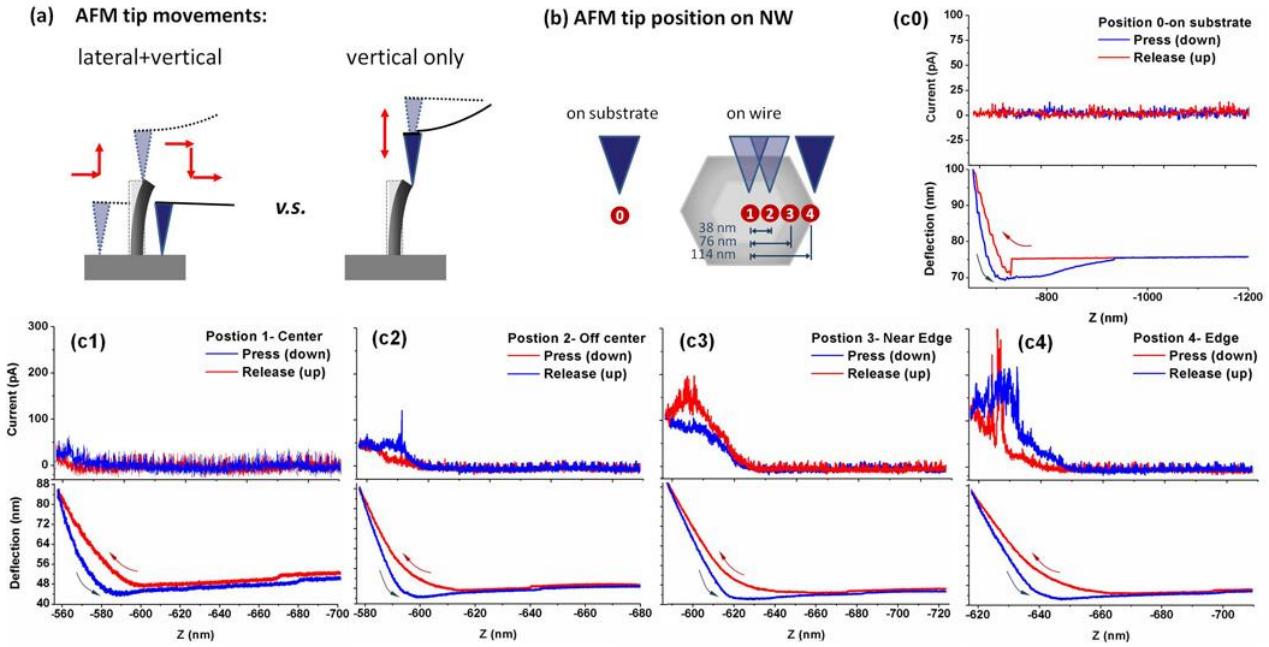

Figure 5 (a) Schematics of single NW bending using cAFM. **(b)** Positions probed **(c0-c4)** Current-Force curves showing the current response (upper) and the deflection of cantilever (lower) as the function of vertical distance of the AFM tip. Recorded without bias applied, and while vertically pressing (red curves) and subsequently withdrawing (blue curves) away from the substrate at various positions (**c0**).

Appendix A. Supplementary material

Additional sections describing data and additional figures. Supplementary data associated with this article can be found in the online version at xxx.

Author information

Corresponding Author

* Email: ximin.he@asu.edu

Notes

The authors declare no competing financial interest.

Acknowledgments

The authors thank Professor Zhonglin Wang (Georgia Institute Technology) for valuable discussion and comments.

References

[1] Y. Cui, C. M. Lieber, Science 291 (2001) 851-853.

[2] Y. Cui, X. Duan, C. M. Lieber, J. Phys. Chem. B 104 (2000) 5213-5216.

[3] H. J. Snaith, G. L. Whiting, B. Sun, N. C. Greenham, W. T. S. Huck, R. H. Friend, Nano Lett. 5 (2005) 1653-1657.

[4] X. Li, L. Basile, B. Huang, C. Ma, J. Lee, I. V. Vlassiouk, A. A. Puretzky, M. Lin, M. Yoon, M. Chi, J. C. Idrobo, C. M. Rouleau, B. G. Sumpter, D. B. Geohegan, K. Xiao, ACS Nano 9 (2015) 8078-8088.

[5] Z. L.Wang, Journal of Physics: Condensed Matter 16 (2004) R829-R858.

[6] T. Makino, Y. Segawa, A. Tsukazaki, A. Ohtomo, M. Kawasaki, Appl. Phys. Lett. 87 (2005) 022101-022101-3.

[7] Ü. Özgür, Y. I. Alivov, C. Liu, A. Teke, M. A. Reshchikov, S. Doğan, V. Avrutin, S. J. Cho, H. A. Morkoç, J. App. Phys. 98 (2005) 041301-041301-3.

[8] P. Ravirajan, A. M. Peiró, M. K. Nazeeruddin, M. Graetzel, D. D. C. Bradley, J. R. Durrant, J. Nelson, J. Phys. Chem. B 110 (2006) 7635-7639.

[9] S. Yamabi, H. Imai, J. Mater. Chem. 12 (2002) 3773-3778.

[10] L. E. Greene, M. Law, D. H. Tan, M. Montano, J. Goldberger, G. Somorjai, P. Yang, Nano Lett. 5 (2005) 1231-1236.

[11] S. C. Rai, K. Wang, Y. Ding, J. K. Marmon, M. Bhatt, Y. Zhang, W. Zhou, Z. L. Wang, ACS Nano 9 (2015) 6419-6427.

[12] X. Wang, J. Song, J. Liu, Z. L. Wang, Science 316 (2007) 102-105.

[13] Y. Qin, X. Wang, Z. L. Wang, Nature 451 (2008) 809-813.

[14] J. Liu, S. Wang, Z. Bian, M. Shan, C. Huang, App. Phy. Lett. 94, (2009) 173107-173107-3.

[15] X. He, F. Gao, G. Tu, D. Hasko, S. Hüttner, U. Steiner, N. C. Greenham, R. Friend, W. Huck, Nano Lett.10 (2010) 1302-1307.

[16] K. M. Coakley, M. D. McGehee, Chem. Mater. 16 (2004) 4533-4543.

[17] J. Slota, X. He, W. Huck, Nano Today, 5 (2010) 231-242.

[18] B. Kannan, K. Castelino, A. Majumdar, Nano Lett. 3 (2003) 1729-1733.

[19] X. He, F. Gao, G. Tu, D. Hasko, S. Huttner, U. Steiner, N. C. Greenham, R. Friend, W. T. S. Huck, Adv. Funct. Mater. 21 (2011) 139-146.

[20] H. Ng, J. Han, T. Yamada, P. Nguyen, Y. P. Chen, M. Meyyappan, Nano Lett. 4 (2004) 1247-1252.

[21] X. He, C. Li, F. Chen, G. Shi, Adv. Func. Mater. 17 (2007) 2911-2917.

[22] S. Xu, N. Adig, S. Ba, T. Desgupta, C. F. Wu, Z. L. Wang, ACS Nano 3 (2009) 1803-1812.

(23) A. I. Hochbaum, R. Fan, R. He, P. Yang, Nano Lett. 5 (2005) 457-460.

[24] Y. Xia, P. Yang, Y. Sun, Y. Wu, B. Mayers, B. Gates, Y. Yin, F. Kim, H. Yan, Adv. Mater. 15 (2003) 353-389.

[25] M. Huang, S. Mao, H. Feick, H. Yan, Y. Wu, H. Kind, E. Weber, R. Russo, P. Yang, Science 292 (2001) 1897-1899.

[26] M. Huang, Y. Wu, H. Feick, N. Tran, E. Weber, P. Yang, Adv. Mater. 13 (2001) 113-116.

[27] W. Liu, F. Xiu, K. Sun, Y. H. Xie, K. L. Wang, Y. Wang, J. Zou, Z. Yang, J. L. Liu, J. Am. Chem. Soc. 132 (2010) 2498-2499.

[28] J. Zhang, L. D. Sun, J. L. Yin, H. L. Su, C. S. Liao, C. H. Yan, Chem. Mater. 14 (2002) 4172-4177.

[29] J. J. Cole, X. Wang, R. J. Knuesel, H. O. Jacobs, Nano Lett. 8 (2008) 1477-1481.

[30] Y. Wei, W. Wu, R. Guo, D. Yuan, S. Das, Z. L. Wang, Nano Lett. 10 (2010) 3414–3419.

[31] K. S. Kim, H. Jeong, M. S. Jeong, G. Y. Jung, Adv. Funct. Mater. 20 (2010) 3055–3063.

[32] S. Xu, Y. Wei, M. Kirkham, J. Liu, W. Mai, D. Davidovic, R. L. Snyder, Z. L. Wang, J. Am. Chem. Soc. 130 (2008) 14958-14959.

[33] L. H. Kaplan, B. K. Bergin, Journal of The Electrochemical Society 127 (1980) 386-395.

[34] X. He, J. Winkel, W. T. S. Huck, Adv. Mater. 21 (2009) 2083-2087.

[35] M. Orban, I. R. Epstein, J. Am. Chem. Soc. 109 (1987) 101-106.

[36] S. S. Lin,; J. H. Song,; Y. F. Lu,; Z. L. Wang, Nanotechnology 20 (2009) 365703.

[37] Y. Gao, Z. Wang, Nano Lett. 9 (2009) 1103-1110.

[38] M. Lu, J. Song, M. Lu, M. Chen, Y. Gao, L. Chen, Z. L. Wang, Nano Lett. 9 (2009) 1223-1227.

[39] J. Song, X. Wang, E. Riedo, Z. L. Wang, Nano lett. 5 (2005) 1954-1958.

[40] Y.W. Heo, L. C. Tien, Y. Kwon, D. P. Norton, S. J. Pearton, B. S. Kang, F. Ren, Appl. Phys. Lett. 85 (2004) 2274-2276.

[41] J. D. Jackson, Classical Electrodynamics, Wiley, Hoboken, 1999.

[42] R. A. Serway, J. W. Jewett, Principles of Physics. Brooks/Cole, Boston, 2006.

[43] J. Volk, T. Nagata, R. Erdélyi, I. Bársony, A. L. Tóth, I. E. Lukács, Z. Czigány, H. Tomimoto, Y. Shingaya, T. Chikyow, Nanoscale Res Lett. 4 (2009) 699-704.

[44] Z. L. Wang, J. H. Song, Science 312 (2006) 242-246.

[45] W. Han, Y. Zhou, Y. Zhang, C. Y. Chen, L. Lin, X. Wang, S. Wang, Z. L. Wang, ACS Nano 6 (2012) 3760-3766.

[46] Z. L. Wang, Adv. Mater. 24 (2012) 1410-1417.

[47] S. Xu, B. J. Hansen, Z. L. Wang, Nat. Commun. 1 (2010) 93.

[48] S. Xu, N. Adig, S. Ba, T. Desgupta, C. F. Wu, Z. L. Wang, ACS Nano 3 (2009) 1803-1812.

[49] I. Horcas, R. Fernández, J. M. Gómez-Rodríguez, J. Colchero, J. Gómez-Herrero, A. M. Baro, J. Rev. Sci. Instrum. 78 (2007) 013705-013705-8.

Graphical Abstract